DYNAMIC SURFACE TOPOGRAPHY: A NEW INTERPRETATION BASED UPON MANTLE FLOW MODELS DERIVED FROM SEISMIC TOMOGRAPHY

A.M. Forte, W.R. Peltier, A.M. Dziewonski, and R.L. Woodward

Reprinted from

Geophysical Research Letters

Volume 20, Number 3, February 1993

GEOPHYSICAL RESEARCH LETTERS, VOL. 20, NO. 3, PAGES 225-228, FEBRUARY 5, 1993

DYNAMIC SURFACE TOPOGRAPHY: A NEW INTERPRETATION BASED UPON MANTLE FLOW MODELS DERIVED FROM SEISMIC TOMOGRAPHY

A.M. Forte[1], W.R. Peltier[2], A.M. Dziewonski[1], and R.L. Woodward[1]

[1]Dept. Earth & Planet. Sci., Harvard University; [2]Physics Dept., University of Toronto

Abstract. The very long wavelength (i.e. in the degree range $\ell = 1$–8) dynamic topography at the Earth's surface, estimated by isostatic reduction of the observed topography, is shown to be in good agreement with the topography predicted by a model of viscous flow in the mantle. This flow model was previously derived by independent consideration of the observed nonhydrostatic geoid and is based upon a recent model of large-scale seismic shear velocity heterogeneity in the mantle. Our estimate (and prediction) of the long wavelength dynamic surface topography reveals significant depressions ($\approx$ 2-3 km) of the continental shields relative to their hydrostatic reference positions.

Introduction

The thermal convective circulation in the Earth's mantle gives rise to viscous normal stresses which act to deflect the Earth's solid surface away from its hydrostatic reference position. Observations of this global-scale dynamic topography are not straightforward because the actual observed surface topography (see Figure 1a) is evidently dominated by the pattern of elevated continents and depressed ocean basins which is due to the isostatic compensation of continent-ocean crustal heterogeneity [e.g. Love, 1911; Jeffreys, 1970]. The first objective of our study is to estimate this isostatic continent-ocean component of the actual surface topography. Given this estimate we then determine the actual dynamic component of the global topography by subtracting the estimated isostatic topography from the observed topography.

The primary objective of our study is to demonstrate that the dynamic topography so estimated also agrees with the long wavelength topography predicted by models of viscous flow in the mantle driven by density contrasts derived from seismic tomographic models of mantle heterogeneity. The importance of this demonstration stems from the fact that the nonhydrostatic geoid predicted by these flow models is very sensitive to the opposing gravitational effects of the flow-induced surface topography and of the internal density contrasts. If the predicted surface topography were to differ significantly from the observed dynamic topography, as suggested previously [e.g. Gurnis, 1990; Cazenave and Lago, 1991], then the previously demonstrated good fits to the nonhydrostatic geoid [e.g. Hager et al., 1985] provided by the viscous flow models would not be physically meaningful. We will examine this important issue by employing a viscous flow model which is based on the recently constructed model $SH8/WM13$ [Woodward et al., 1992] of large-scale shear-velocity heterogeneity in the mantle. This flow model was originally constrained to provide a good match to the observed long wavelength nonhydrostatic geoid [Forte et al., 1992] and was derived independently of any information concerning the actual dynamic topography at the Earth's surface.

Previous observational studies of the dynamic surface topography [e.g. Cazenave et al., 1989; Colin and Fleitout, 1990; Cazenave and Lago, 1991] have confined themselves to the analysis of the bathymetry of the sea floor. Such studies have usually defined the 'dynamic' component of this bathymetry to be the residual topography obtained by removing the $[age]^{1/2}$-variation associated with the cooling oceanic lithosphere. In this study we will not make any distinction between this age-dependence of the oceanic bathymetry and the dynamic topography. The $[age]^{1/2}$-variation of sea-floor topography will be implicitly included in our predictions of dynamic surface topography since the model of seismic heterogeneity employed here clearly contains a similar age-dependence of seismic velocities in the upper-most suboceanic mantle [see Fig. 2 in Su et al., 1992]. In contrast to previous observational studies of dynamic surface topography we shall consider its variation on a global scale. This requires that we consider not only the dynamic topography in the ocean basins but also that in continental regions. As we shall see, the dynamic topography in continental regions is quite large and contributes significantly to the global signal.

Paper number 93GL00249
0094-8534/93/93GL-00249$03.00

Isostatic Surface Topography

Various specifications of the isostasy principle have been formulated [e.g. Love, 1911; Garland, 1977; Dahlen, 1982] and they all yield, to first-order accuracy, the well known local condition of constant total mass (down to the so-called depth of 'compensation') in any given unit-area vertical column at the surface. We shall apply this formulation of isostasy to the model of continent-ocean heterogeneity illustrated schematically in Figure 2. In this model we adopt the crustal densities and crustal layers identified in the $PEM-C$ and $PEM-O$ models of Dziewonski et al. [1975] in which the continental regions are assumed to consist of an upper crust (with density $\rho_{uc} = 2.72 Mg/m^3$) and a lower crust (with density $\rho_{lc} = 2.92 Mg/m^3$) while the oceanic regions consist of a water layer (with density $\rho_w = 1.02 Mg/m^3$) overlying a single-layer crust (with density $\rho_{oc} = 2.85 Mg/m^3$). The continental and oceanic crusts both overly a mantle with a near-surface density $\rho_m = 3.3 Mg/m^3$. The application of the isostasy principle thus reduces to the determination of the radial locations (see Figure 2) of the solid surface, the ocean surface, the mid-crust boundary, and the Mohorovičić ('moho') discontinuity in the continental and oceanic regions which ensure that the total mass in any unit-area vertical column is constant.

To begin we follow Woodhouse and Dziewonski [1984] and employ their continent-ocean function $C(\theta, \varphi)$, derived from the surface regionalization of Mauk [1977], to describe the surface distribution of continents and oceans. This continent-ocean function has zero mean (i.e. the $\ell = 0, m = 0$ spherical harmonic component vanishes) thus ensuring that we neither alter the density nor the locations of the material boundaries in the spherically symmetric reference Earth model. We note that in continental regions $C(\theta, \varphi) = C_c$ (≈ 0.66) and in oceanic regions $C(\theta, \varphi) = C_o = C_c - 1$. We find that the field $5.18 C(\theta, \varphi)$ $[km]$ provides the best least-squares fit to the observed long wavelength surface topography (in the degree range $\ell = 1$–8) and explains 92% of its variance. This result suggests that the continent-ocean function will provide an excellent

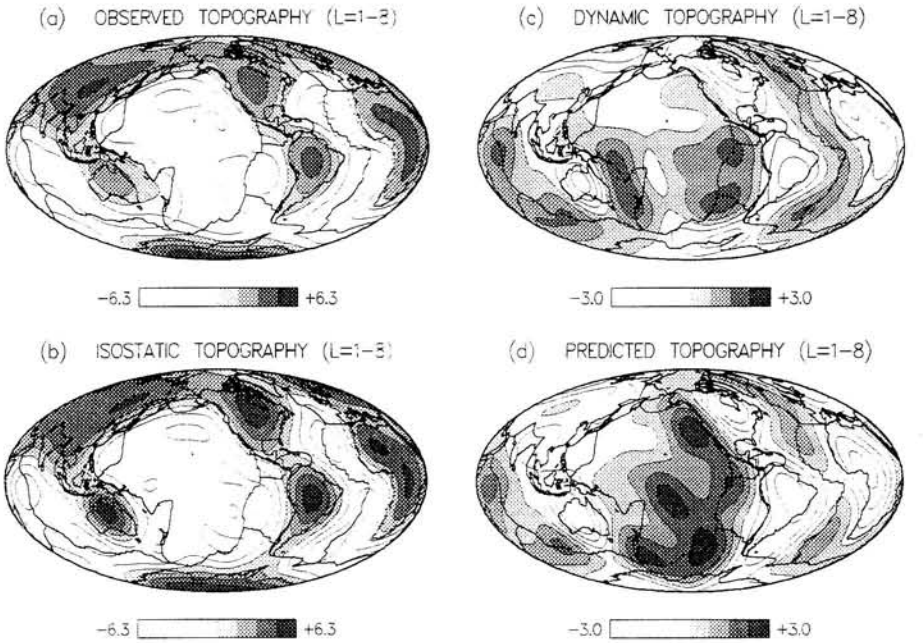

Fig. 1. (a) The solid surface topography derived from the ETOPO5 data base [National Geophysical Data Center, 1986] in the spherical harmonic degree range $\ell = 1-8$. The contour interval is 1.575 km. (b) The isostatic solid surface topography, given by equation (9) in the text, in the degree range $\ell = 1-8$. The contour interval is 1.575 km. (c) The residual dynamic component of the topography obtained by subtracting the field in (b) from the field in (a). The contour interval is 0.75 km. (d) The flow-induced solid surface topography, in the degree range $\ell = 1-8$, predicted with model $SH8/WM13$ [Woodward et al., 1992] using the viscosity profile in Figure 3a and $\partial ln\rho/\partial lnv_S$ in Figure 3b. The contour interval is 0.75 km.

basis for describing the long wavelength isostatic crustal heterogeneity and boundary deflections.

Following the notation in Figure 2 we write the perturbation to the outer radius of the ocean layer ($r = r_e$) as

$$\delta r_e(\theta,\varphi) = (h_c + h_w)C(\theta,\varphi), \tag{1}$$

the perturbation to the radius of the solid surface ($r = a$) as

$$\delta a(\theta,\varphi) = (r_e - a + h_c + h_o)C(\theta,\varphi), \tag{2}$$

the perturbation to the radius of the mid-crust boundary ($r = r_{mid}$) as

$$\delta r_{mid}(\theta,\varphi) = -(d + H_o)C(\theta,\varphi), \tag{3}$$

and the perturbation to the radius of the moho ($r = r_{moho}$) as

$$\delta r_{moho}(\theta,\varphi) = -(r_{mid} - r_{moho} + H_o + H_c)C(\theta,\varphi). \tag{4}$$

The condition of constant mass per vertical column thus reduces to the following expression

$$\rho_{uc}\Delta_{uc} + \rho_{lc}\Delta_{lc} = \rho_w\Delta_w + \rho_{oc}\Delta_{oc} + \rho_m\Delta_m, \tag{5}$$

where $\Delta_{uc} = r_e - r_{mid} + (h_c + h_w + d + H_o)C_c$ is the thickness of the continental upper crust, $\Delta_{lc} = r_{mid} - r_{moho} + (r_{mid} - r_{moho} + H_c - d)C_c$ is the thickness of the continental lower crust, $\Delta_w = r_e - a - (r_e - a + h_o - h_w)C_o$ is the thickness of the ocean layer, $\Delta_{oc} = a - r_{mid} + (r_e - a + h_c + h_o + d + H_o)C_o$ is the thickness of the oceanic crust , and $\Delta_m = r_{mid} - r_{moho} + H_o + H_c$ is the thickness of the mantle wedge beneath the oceanic crust. It is evident in Figure 2 that the ocean layer is effectively pinched to zero thickness over the continents and thus

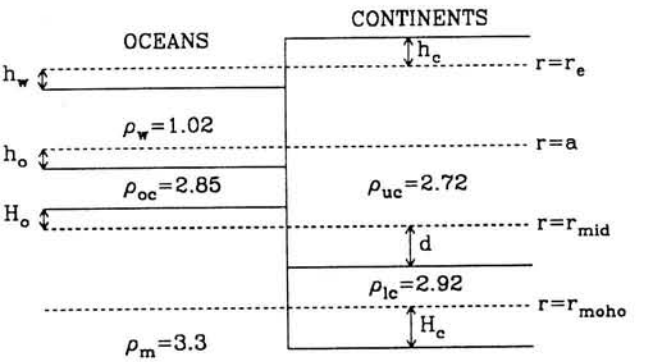

Fig. 2. Schematic representation of the continent-ocean crustal heterogeneity model. The indicated densities (in Mg/m^3) are taken from PEM [Dziewonski et al., 1975]. The dashed horizontal lines indicate the locations of the spherical boundaries in the radial reference model (e.g. in PREM [Dziewonski and Anderson, 1981] $r_e = 6371km$, $a = 6368km$, $r_{mid} = 6356km$, $r_{moho} = 6346.6km$). The solid horizontal lines indicate the isostatically-defined (see text) locations of these horizons.

$$\Delta_w = (r_e - a)/C_c \tag{6}$$

which is simply the condition that the spherically averaged thickness of the ocean layer be the same as that in the radial reference model (e.g. PREM [Dziewonski and Anderson, 1981]). Similarly, the lower crust beneath the continents is pinched to zero thickness below the oceans and thus

$$\Delta_{lc} = -(r_{mid} - r_{moho})/C_o \tag{7}$$

which is the condition that the spherically averaged thickness of the lower crust be the same as that in the radial

reference model. Finally the condition that the spherically averaged thickness of the continental upper crust and oceanic crust be the same as that of the upper crust of the radial reference model yields

$$\Delta_{oc}(C_c) + \Delta_{uc}(-C_o) = a - r_{mid}. \quad (8)$$

As pointed out in Dziewonski et al. [1975] this spherical averaging of layer thicknesses also makes sense from the viewpoint of the effective averaging provided by multiply-reflected propagating seismic waves (which is thus reflected in the normal-mode eigenperiods of the radial reference model). Equations (5)-(8) are not sufficient to provide unique constraints on each of the layer thicknesses in Figure 2. The final constraint may be obtained by simply adopting the thickness of the continental upper crust $\Delta_{uc} = 20km$ in the $PEM-C$ model of Dziewonski et al. [1975]. We thus find (algebra not shown here) that $(r_e - a + h_c + h_o) = 6.88km$ and the expression for the isostatic surface topography in (2) becomes

$$\delta a(\theta,\varphi) = 6.88C(\theta,\varphi)\ [km]. \quad (9)$$

In Figure 1b we show the long wavelength component of the isostatic surface topography in (9) and a comparison with the actual long wavelength topography in Figure 1a, derived from the ETOPO5 data base [National Geophysical Data Center, 1986], immediately shows a close correspondence. This correspondence confirms the importance of the contribution of isostatically compensated continent-ocean crustal heterogeneity to the observed surface topography.

Haxby and Turcotte [1978] employ a model of continent-ocean crustal heterogeneity (see their Figure 6) which provides a good match to the observed geoid variation across passive continental margins. In their model the continental lower crust is effectively a continuation of the oceanic crust and the continental upper crust is pinched to zero thickness in the ocean basins. According to this model we should rewrite the perturbation of the mid-crust boundary, in eq. (3), as

$$\delta r_{mid}(\theta,\varphi) = (r_{mid} - a - d + h_o)C(\theta,\varphi)\ . \quad (10)$$

The pinching of the continental upper crust requires, in analogy to eq. (7), that

$$\Delta_{uc} = -(a - r_{mid})/C_o\ . \quad (11)$$

In analogy to eq. (8) we have the following averaging of the continental lower crust and the oceanic crust:

$$\Delta_{oc}(C_c) + \Delta_{lc}(-C_o) = r_{mid} - r_{moho}\ . \quad (12)$$

If we now employ the crustal densities in Haxby and Turcotte [1978] and choose $\Delta_{oc} = 7km$ [Soller et al., 1982] we find that the isostatic solid-surface topography is now given by

$$\delta a(\theta,\varphi) = 8.11C(\theta,\varphi)\ [km]\ . \quad (13)$$

In Figure 1c we show the long wavelength dynamic surface topography which is obtained by subtracting the isostatic topography in eq. (9) from the observed topography in Figure 1a. If instead we subtract the isostatic topography given by eq. (13), we obtain a dynamic topography (not shown here) whose pattern is strongly correlated to that in Figure 1c and whose (root-mean-square) amplitude is 40% larger. This amplitude difference may be regarded as a measure of the uncertainty in the estimated dynamic topography in Figure 1c.

Clearly we haven't made an exhaustive analysis of all possible crustal models and this raises the question of whether there exists an isostatic model with a surface topography nearly identical to that in Figure 1a. We find from a direct inverse analysis that such a model [yielding $\delta a(\theta,\varphi) = 5.2C(\theta,\varphi)$] arises only by making the implausible assumption of an almost undifferentiated crust (i.e. $\rho_{uc} \doteq \rho_{oc}$).

Dynamic Surface Topography

The density perturbations in the mantle which are derived from the models of global seismic heterogeneity have been shown to provide rather realistic predictions predictions of important convection-related observables such as the nonhydrostatic geoid, tectonic plate motions, and core-mantle boundary topography [e.g. Hager et al., 1985; Forte and Peltier, 1987,1991]. The relevant viscous flow theory has been described in detail in Richards and Hager [1984], Ricard et al. [1984], and Forte and Peltier [1987,1991]. Employing this theory we may derive the kernel functions $A_\ell(r)$ which relate the spherical harmonic coefficients of the flow-induced surface topography δa_ℓ^m to the radially varying coefficients of the driving density contrasts $\delta\rho_\ell^m(r)$ as follows:

$$\delta a_\ell^m = \frac{1}{\Delta\rho_{mo}} \int_b^a A_\ell(r)\delta\rho_\ell^m(r)dr, \quad (14)$$

in which $\Delta\rho_{mo} = 2.2Mg/m^3$ is the density jump across the mantle-ocean boundary. The behaviour of the topography kernels $A_\ell(r)$ depends on the radial profile of relative (i.e. nondimensional) viscosity in the mantle.

The predicted nonhydrostatic geoid is quite sensitive to the depth variation of relative viscosity [e.g. Richards and Hager, 1984] and in Figure 3a we show the relative viscosity profile inferred by Forte et al. [1992] from their modeling of the geoid data using the shear-velocity heterogeneity model of Woodward et al. [1992]. In Figure 3b we show the corresponding proportionality between shear velocity and density perturbations, $\partial ln\rho/\partial lnv_S$, which has been inferred by least squares fitting to the nonhydrostatic geoid data. The $\partial ln\rho/\partial lnv_S$ values so inferred are: 0.11 from 0-400 km depth, 0.37 from 400-670 km depth, and a linear variation (a-priori choice) from 0.22 at the top of the lower mantle to 0.15 at the core-mantle boundary. In Figure 3c we show the surface topography kernels for the

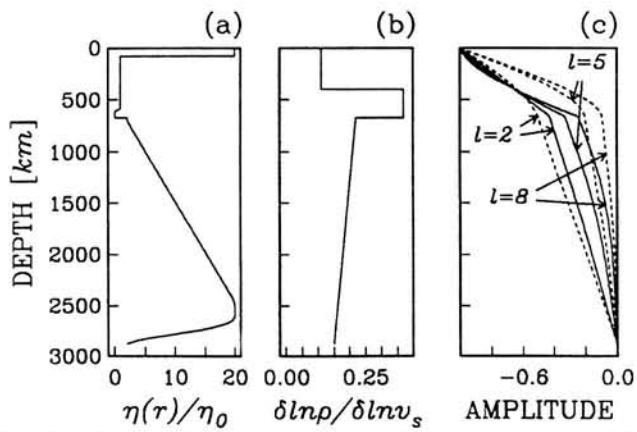

Fig. 3. (a) The relative viscosity profile inferred from geoid modeling by Forte et al. [1992]. (b) The proportionality between perturbations of shear velocity and density, $\partial ln\rho/\partial lnv_S$, inferred by least squares fitting to the nonhydrostatic geoid data [Forte et al., 1992]. (c) The dynamic surface topography kernels $A_\ell(r)$, defined in equation (10) in the text. The solid curves are the kernels calculated for the viscosity profile in (a) and the dashed lines are the kernels calculated for a two-layer viscosity profile with a factor of 30 viscosity jump at 670 km depth.

viscosity profile in Figure 3a calculated with the gravitationally consistent compressible-flow theory of Forte and Peltier [1991]. It is important to appreciate that while the predicted geoid is quite sensitive to the depth variation of mantle viscosity, the predicted surface topography is (by comparison) much less sensitive. To illustrate this point we also show in Figure 3c the surface topography kernels for a two-layer viscosity profile with a factor of 30 jump at 670 km depth. We see therefore that the dynamic surface topography in Figure 1c provides good constraints on the amplitude and spatial distribution of density perturbations in the upper mantle.

In Figure 1d we now show the long wavelength flow-induced solid surface topography predicted, according to (14), by convolving the field of density perturbations derived from model $SH8/WM13$ of Woodward et al. [1992] (using $\partial ln\rho/\partial lnv_S$ in Figure 3b) with the topography kernels in Figure 3c which correspond to the viscosity profile in Figure 3a. It is evident from these kernels that the predicted surface topography is dominated by the contribution from upper-mantle density contrasts. The root-mean-square amplitude of the topography contribution from density contrasts in the top 400 km of the mantle is 0.7 km, from 400–670 km it is 0.5 km, and from the lower mantle it is 0.4 km. A comparison of Figures 1c and 1d reveals a good agreement, both spatially and in terms of absolute amplitude. In particular, both maps show a clear pattern of elevated mid-ocean ridges (which has a remarkably broad spatial extent in the Pacific) and striking topographic depressions centred on the ancient continental shields.

Conclusion

The original motivation for this study came from the discrepancy previously suggested between the amplitudes of past inferences of dynamic topography and the topography predicted by viscous flow models of the mantle [e.g. Gurnis, 1990; Cazenave and Lago, 1991]. As emphasized in the Introduction, the resolution of this issue is of great importance because it bears directly on the validity of the viscous-flow theory which has so far been employed to model the long wavelength nonhydrostatic geoid. Our analysis has now verified that viscous flow models which provide a good match to the long wavelength geoid may also agree with the estimated global dynamic topography shown in Figure 1c. This agreement is rather encouraging, especially in view of the important simplifying assumptions (e.g. spherically-symmetric viscosity) inherent in the viscous flow models and also the approximation made in deducing the dynamic topography shown in Figure 1c (i.e. assuming that all continents have equal thickness and density).

A new and important outcome of this study is the inference of the significant long-wavelength dynamical depressions ($\approx$ 3 km) of the continental cratons relative to their hydrostatic reference level. Such depressions are important because their gravitational effect seems to be responsible for the negative free air gravity anomalies observed over centres of Pleistocene deglaciation such as Hudson Bay [Peltier et al., 1992]. We may understand these continental depressions in terms of the dynamic 'suction' which develops as a consequence of the downwelling flow driven by the density contrasts associated with the deep high-velocity 'roots' of the continents in model $SH8/WM13$.

Acknowledgements. We thank Wei-jia Su for his 'GEOMAP' program used in the preparation of Figure 1. This work has been supported by a Canadian NSERC postdoctoral fellowship to A.M.F., by NSERC grant A9627 (W.R.P.) and by NSF grant EAR90-05013.

References

Cazenave, A., A. Souriau, and K. Dominh, Global coupling of Earth surface topography with hotspots, geoid and mantle heterogeneities, *Nature*, *340*, 54-57, 1989.

Cazenave, A., and B. Lago, Long wavelength topography, seafloor subsidence and flattening, *Geophys. Res. Lett.*, *18*, 1257-1260, 1991.

Colin, P., and L. Fleitout, Topography of the ocean floor: Thermal evolution of the lithosphere and interaction of deep mantle heterogeneities with the lithosphere, *Geophys. Res. Lett.*, *17*, 1961-1964, 1990.

Dahlen, F.A., Isostatic geoid anomalies on a sphere, *J. Geophys. Res.*, *87*, 3943-3947, 1982.

Dziewonski, A.M., A.L. Hales, and E.R. Lapwood, Parametrically simple Earth models consistent with geophysical data, *Phys. Earth Planet. Inter.*, *10*, 12-48, 1975.

Dziewonski, A.M., and D.L. Anderson, Preliminary reference Earth model, *Phys. Earth Planet. Inter.*, *25*, 297-356, 1981.

Forte, A. M., and W.R. Peltier, Plate tectonics and aspherical Earth structure: The importance of poloidal-toroidal coupling, *J. Geophys. Res.*, *92*, 3645-3679, 1987.

Forte, A.M., and W.R. Peltier, Viscous flow models of global geophysical observables. I. Forward problems, *J. Geophys. Res.*, *96*, 20,131-20,159, 1991.

Forte, A.M., A.M. Dziewonski, and R.L. Woodward, Aspherical structure of the mantle, tectonic plate motions, nonhydrostatic geoid, and topography of the core-mantle boundary, in *Dynamics of the Earth's Deep Interior and Earth Rotation*, J.L. LeMouël, ed., AGU Geodyn. Ser., in press, 1992.

Garland, G.D., *The Earth's Shape and Gravity*, Pergamon Press (Oxford), 1977.

Gurnis, M., Bounds on global dynamic topography from Phanerozoic flooding of continental platforms, *Nature*, *344*, 754-756, 1990.

Hager, B.H., R.W. Clayton, M.A. Richards, R.P. Comer, and A.M. Dziewonski, Lower mantle heterogeneity, dynamic topography and the geoid, *Nature*, *313*, 541-545, 1985.

Haxby, W.F., and D.L. Turcotte, On isostatic geoid anomalies, *J. Geophys. Res.*, *83*, 5473-5478, 1978.

Jeffreys, H., *The Earth*, 5th ed., Cambridge University Press (New York), 1970.

Love, A.E.H., *Some Problems in Geodynamics*, Cambridge University Press, 1911.

Mauk, F.J., A tectonic based Rayleigh wave group velocity model for prediction of dispersion character through ocean basins, Ph.D. Thesis, Univ. of Mich., Ann Arbor, 1977.

Peltier, W.R., A.M. Forte, J.X. Mitrovica, A.M. Dziewonski, Earth's gravitational field: Seismic tomography resolves the enigma of the Laurentian anomaly, *Geophys. Res. Lett.*, *19*, 1555-1558, 1992.

Ricard, Y., L. Fleitout, and C. Froidevaux, Geoid heights and lithospheric stresses for a dynamic Earth, *Ann. Geophys.*, *2*, 267-286, 1984.

Richards, M.A., and B.H. Hager, Geoid anomalies in a dynamic Earth, *J. Geophys. Res.*, *89*, 5987-6002, 1984.

Soller, D.R., R.D. Ray, and R.D. Brown, A new global crustal thickness map, *Tectonics*, *1*, 125-149, 1982.

Su, W.-J., R.L. Woodward, and A.M. Dziewonski, Deep origin of mid-ocean ridge seismic velocity anomalies, *Nature*, *360*, 149-152, 1992.

Woodhouse, J.H., and A.M. Dziewonski, Mapping the upper mantle: Three dimensional modeling of Earth structure by inversion of seismic waveforms, *J. Geophys. Res.*, *89*, 5953-5986, 1984.

Woodward, R.L., A.M. Forte, W.-J. Su, A.M. Dziewonski, Constraints on the large-scale structure of the Earth's mantle, in *Chemical Evolution of the Earth and Planets*, Takahashi et al., eds., *J. Geophys. Res.*, in press, 1992.

A.M. Dziewonski, A.M. Forte, R.L. Woodward, Dept. of Earth and Planet. Sci., 20 Oxford St., Harvard University, Cambridge, MA 02138

W.R. Peltier, Dept. of Physics, University of Toronto, Toronto, Canada M5S 1A7

(Received: July 22, 1992;
Revised: November 10, 1992;
Accepted: January 5, 1993.)